# 30330 Image Analysis with Microcomputer

Project report

by

Katleen Blanchet s150798
Titouan Boulmier s150810

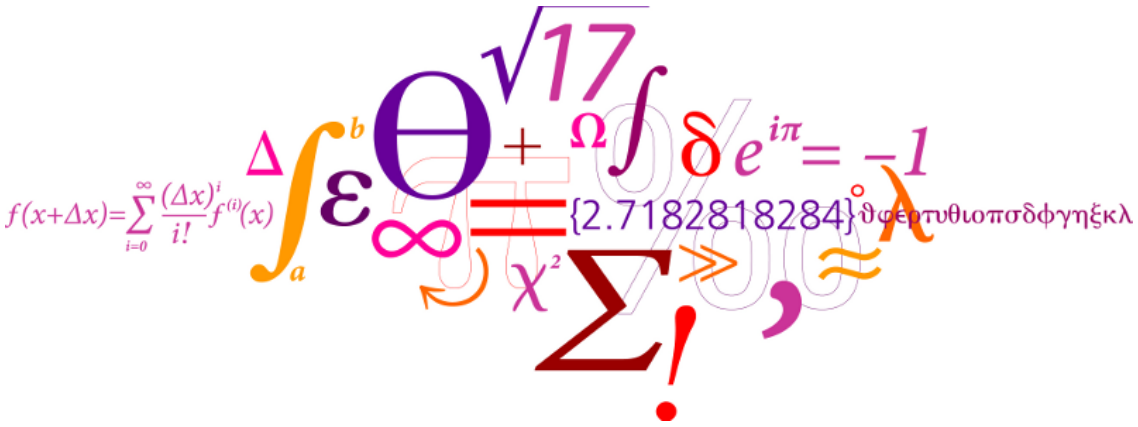


November 25, 2015

Technical University of Denmark
Department of Electrical Engineering

# Contents

# Introduction

# Part 1

# Problem formulation and delimitation

## 1.1 Problem formulation

In this report, we assume that we would like to send a rover on Mars, capable of communicating with Earth. Self-powered by solar panels, it will land at latitude 50° where it could get enough sunlight to recharge its lithium batteries. It is provided with an arm whose hand is replaced with a camera (see figure 1.1). The latter will be used by scientists to observe relevant rocks to study. In order to accomplish this mission, once a stone is designed, the camera must be able to keep it in focus, despite the wind, the movement of the robot or any other perturbation. This implies a real time image analysis to be able to rectify the position of the camera. As a robust method is needed to maintain the stone in front of the arm, the identification of patterns should be completed by carrying out a 3D map of the surface. A luminous source should then be added to the rover to be projected on the surface containing the rock and detected by the camera.

This luminous source must be powerful enough to outshine the sunlight during the day, notwithstanding that the energy needed to make it work has to be negligible compared to the amount provided to the rover. Moreover, the characteristics of the camera need to be perfectly adapted to Mars, as once the rover has landed on the red planet, it would be impossible to adjust it.

Will it be feasible to design such an embedded system, composed of a camera, a luminous source and algorithms, capable of keeping a rock in focus thanks to a 3D map, for an application on Mars soil?

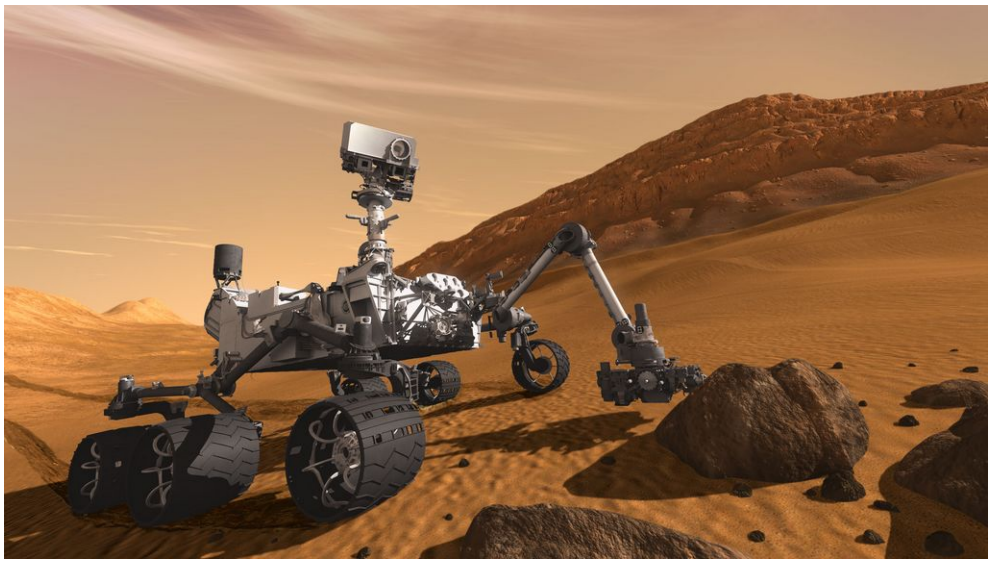

Figure 1.1: Curiosity Rover with an embedded camera on a arm [5]

## 1.2 Problem delimitation

In order to design the rover's camera which will be used to study rocks and to implement a robust algorithm to carry out a 3D map of the rock's surface, different characteristics of Mars and of the target need to be specified. However, as all of them cannot be taken into account, some simplifications and choices will be assumed.

**Mars delimitation**

Plenty of missions on Mars have been realized and a great deal of data has already been gathered. Nevertheless, even if some of them will be used to designed our system, others will be simplified or even ignored. The first simplification concern the atmosphere of Mars. Indeed, even if its composition is now well know, it will be assumed that the dirt on the surface Mars plus the different layers of the atmosphere absorb, or scatter, 10% of the solar energy. Moreover, the influence on the image acquisition that the dirt between the target and the camera could have will not be taken into account. The second reduction cover the temperature. Indeed, even if it can reach -143°C during winter, 27°C during summer and have around 60°C variations between daytime and nighttime[6], we will assume that the CCD sensor works well all the time.

**Target delimitation**

Regarding the target, that is to say the part of the rock being studied, it is supposed to :

- be vertical;
- not exceed 2*2 meters

- have an area between 0.1 and 1 square meters;
- have a relief less than meters.

**Camera delimitation**

Then, regarding the camera which is designed during this study, it is presumed to :

- be between one and two meters far from the target;
- be right in front of the target, that is to say that the angle between the normal of the target's surface and the focal axis of the camera is 0°;
- be able to capture the image of a target of 2 meters height maximum.

The different characteristics of target and the camera are represented figure 1.2

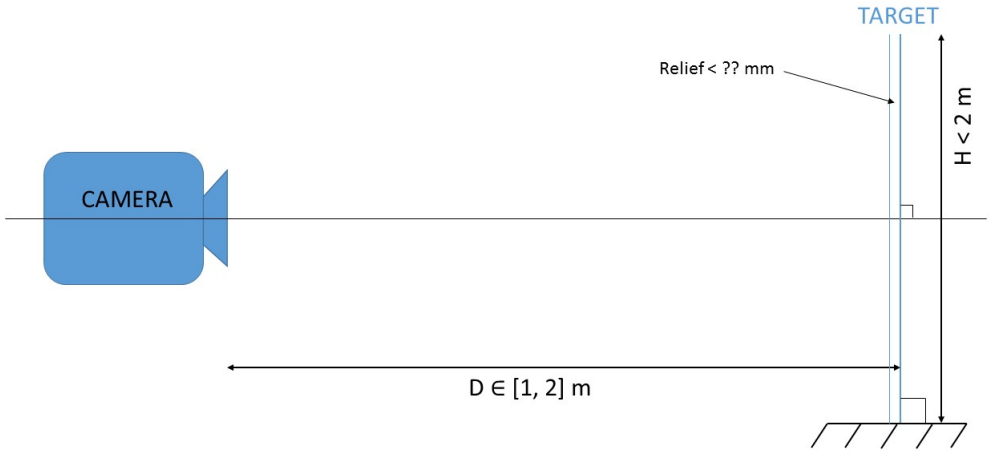


Figure 1.2: Schema of the scene

# Part 2

# Theory Section

## 2.1 Mars Features

### 2.1.1 Albedo

Mars surface is covered by sand and volcanic rocks. The first purpose of this project is to allow scientists to examine these rocks through the camera. To achieve it, it is needed to know their characteristics, especially their albedo. As a reminder, the albedo is the fraction of incident light which is reflected from a surface. We can assume that the power reflection of Martian rocks is the same than on Earth. Then, to cover a wild range of rocks, the albedos of a black and of a white stone would be considered. Charcoal, as a dark rock, is a powerful absorber of the sun radiation, with an albedo around 0.05. On the contrary, chalks are poor absorbers and their albedo reach 0.45 according to [3]. In the following parts of the report, it will be taken for granted that Martian rocks have an albedo between 5 and 45%.

### 2.1.2 Laser

In order to carry out a 3D mapping of the target, the system needs a light source to project points which will be used by the 3D mapping algorithm. In this section, the source of light will be designed.

First of all, the green has been chosen as color of the light source. Indeed, in order to detect easily the points projected on the target, a distinctive color should be used. As we can see figure 2.1, the CCD selected for the camera has the best quantum efficiency for a wavelength around 510 $nm$, which means that the green is the color that is the best recorded by the camera. Secondly, as the surface on Mars is mainly orange, red and brown, this color should stand out.

Then, as only 300 $mW$ are available to aliment the light source and a lot of lightning energy is needed to outshine the sunlight, a LED has been chosen. Indeed,

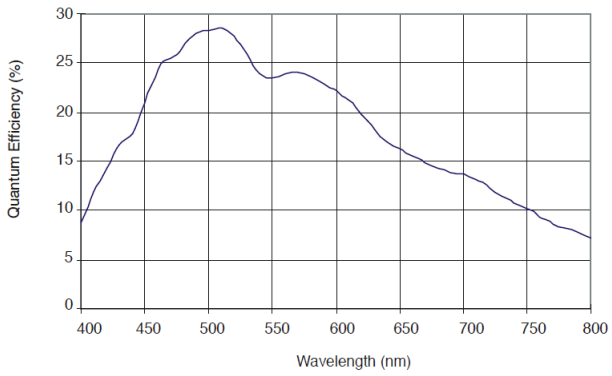


Figure 2.1: Quantum efficiency versus wavelength of the CCD

LEDs have great energy performances. The properties of the chosen LED can be seen in Annex A. Note that the use of a laser have been studied, but the energy cost would have been too expensive. Moreover, even if we cannot obtained a coherent light, as a laser do, with a LED, it is still feasible to obtain a monochromatic and directional light. Thus, we will assume that the LED can bring enough light (proof in part on Signal Noise Ratio**??**). Then, as the 3D mapping algorithm needs a grid of points, the LED cannot be used in its present condition. Moreover, lot of light would be lost without an optic system. Thus, a system has been designed to concentrate the luminous beams of the LED and to transform the continuous light into a grid of point. The system uses a lens and a grid (Figure 2.2).

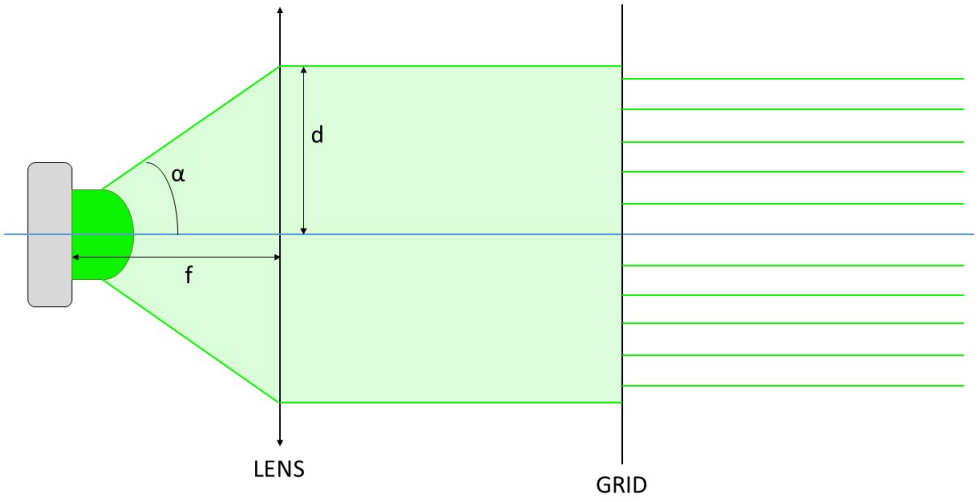


Figure 2.2: schema of the LED system

As the LED has a diffusion angle of 30°'Annex A), the lens needs to be close enough to collect all the light beams of the LED to avoid losses of energy. In order

to capture as much light as possible, the diameter of the lens should follow (2.1).

$$d = f \tan \alpha \tag{2.1}$$

with

$\alpha = \dfrac{30}{2} = 15°$, the half of the diffusion angle.

$f$, the focal length of the lens

Moreover, it should be pointed that there is a loss of energy because of the lens and the grid. We will assume that the energy loss coefficient of the lens is 0.5 and the one of the grid is 0.3.

# Part 3

# Development

## 3.1 Scene Analysis

In order to design the camera and find its characteristics, a scene analysis have to be carried out. Our study is based on the MER (Mars Exploration Rover) cameras properties [4]. To begin with, we choose an image sensor.

### 3.1.1 CCD

The Charge Coupled Device (CCD) is commonly more sensitive to light than its counterpart, the CMOS (Complementary Metal Oxide Semiconductor). Moreover, in the near infrared CCD appears to have a better response. Since Mars has a reddish color, it seems more accurate to select the CCD detector.

As scientists will need to discern the details of rocks, the resolution should be around the megapixel. Taking into account the cost, which will increase with the resolution, and the time of computation for an image with too many pixels, 1024 x 1024 seems to be an acceptable compromise.

Finally, the last element to consider is the pixel size. A trade-off have to be found between having a higher resolution (smaller pixels) and more sensitivity (larger pixels). All the camera of the MER mission were conceived with a pixel size of 12 x 12 $\mu m$ for a resolution of 1024 x 1024. It was decided to comply with that value.

For the next parts of this report, we will use the data sheet of the FTT1010M CCD image sensor as a basis for our calculations which will require CCD details.

### 3.1.2 Field of View

According to the book [1], the Field of View (FoV) "is the angle of the cone of directions encompassed by the scene that is being images". This solid angle is needed to compute the focal length the camera should have.

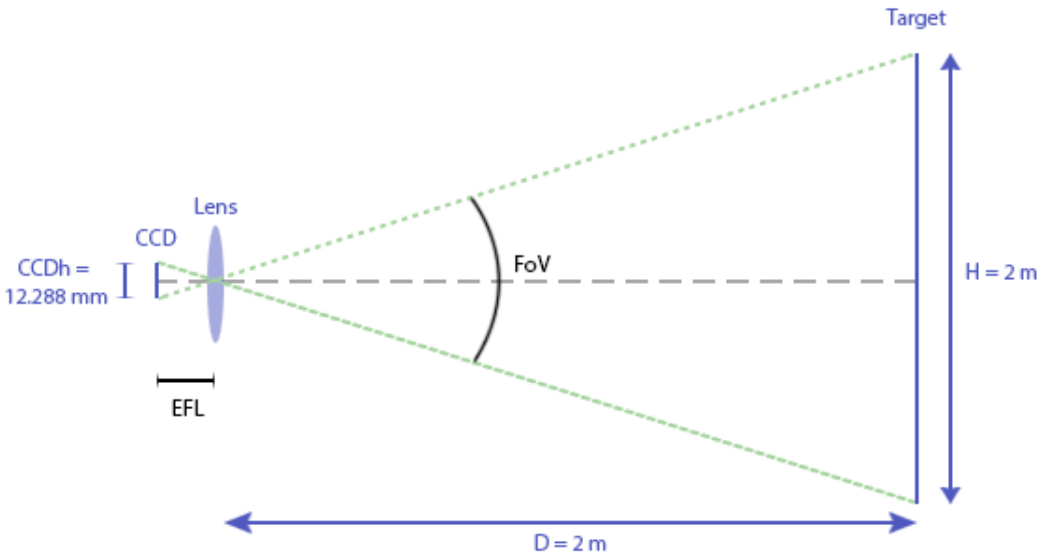


Figure 3.1: Field of View and Effective Focal Length

A simple relationship between the distance lens-target, the size of the target and the FoV can be deduced from the detailed diagram 3.1:

$$tan(\frac{FoV}{2}) = \frac{1}{2} \times \frac{H}{D}$$

We derive and get

$$\frac{FoV}{2} = atan(\frac{1}{2} \times \frac{H}{D})$$

Numerically, with our problem delimitation, the Field of View is equal to $26.6° \times 26.6°$.

### 3.1.3 Focal Length

Thanks to the previous diagram, the Effective Focal Length (EFL) can also be determined:

$$EFL = \frac{1}{2} \times \frac{CCDh}{tan(\frac{FoV}{2})} = 12.29\ mm$$

where $CCDh$ is the image section of the CCD according to the data sheet.

In order to get the real focal length, we choose $rf = 1\ m$ for the distance of focus of the camera.

$$f = \frac{1}{\frac{1}{rf} + \frac{1}{EFL}} = 12.14\ mm$$

### 3.1.4 Aperture

To determine the diameter of the aperture, several criteria have to be accounted for. If the diameter is too small, the sharpness of the image will decrease due to the diffraction effect. In fact, at large aperture, the diffracted light is negligible compared to the total amount of light entering the system. On the other hand, we should also consider the Depth of Field (FoV). We need to insure that it is big enough to allow us to see the whole target on the image. The relationship between the DoF and the diameter is inversely proportional. That means that if we increase the diameter, we will lessen it. The Circle of Confusion (CoC), linked to the DoF is also a factor to take into consideration for the choice of the diameter. According to Wikipedia [7] It corresponds to "an optical spot caused by a cone of light rays from a lens not coming to a perfect focus when imaging a point source". The smaller the CoC is, which corresponds to a better focus, the bigger is the DoF, and also the smaller is the diameter.

As the behaviour of the depth of field and of the circle of confusion runs counter to the diffraction one, a trade-off has to be found.

These formula are used to calculate the Diameter of Confusion (DoC) and the diffraction spot:

$$DoC = Dsr \cdot \frac{|r - rf|}{r} \cdot \frac{f}{rf - f}$$

where $Dsr$ is the diameter of the aperture

$$DiffractionSpot = 2 \cdot EFL \cdot tan(1.22 \cdot \frac{lambda}{Dsr})$$

where $lambda$ is a wavelength of the sunlight

In the delimitations, it is assumed that the wavelengths of the sunlight belong to [400 800] nm. To settle on a diameter, the diameter of confusion and the diffraction spot were computed for diameters varying from 1 mm to 5 mm and wavelengths from 400 nm to 800 nm. The results are shown graphically in figure 3.2. As the diameter of confusion cannot be bigger than the height of a pixel, the line corresponding to 12 $\mu m$ was also added to the graphic. In order to have the best trade-off, that is to say all the curves under 12 $\mu m$, we have chosen a effective lens entrance aperture $Dsr$ equal to 1.9 $mm$, corresponding to $DoC = 0.0117$ $mm$.

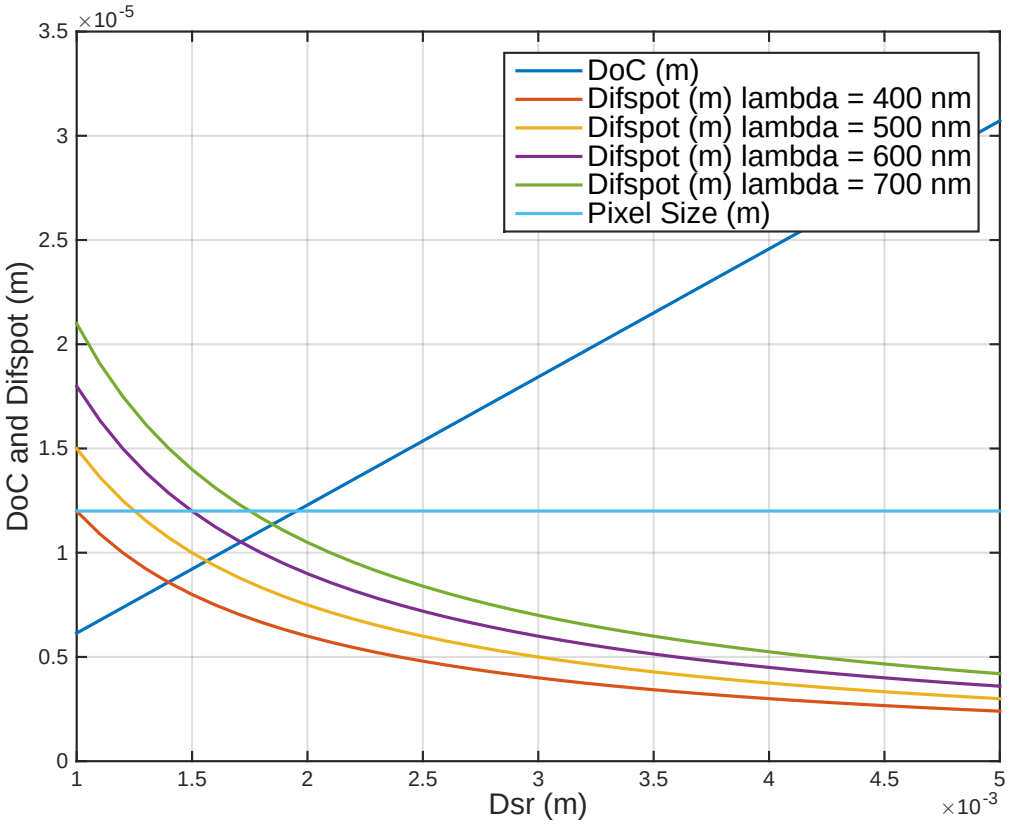


Figure 3.2: Diameter of confusion and diffraction spots as a function of the diameter

The circle of confusion can be deduced:

$$CoC = DoC \cdot m \qquad where\ m = \frac{EFL}{rf}$$

and then:

$$DoF = \frac{2\frac{f}{Dsr}CoC(m+1)}{m^2 - (\frac{CoC}{Dsr})^2} = 12.29\ mm$$

That means that the roughness of the rock analysed cannot be more than $\frac{DoF}{2} = 6.14\ mm$ since we could not see the whole rock if not, and the 3D map will then be flawed.

### 3.1.5 Irradiance

First of all, the irradiance $F$ of the light from the sun falling at the top of the atmosphere of Mars can be calculated as following : Conservation of energy :

$$4\pi R_{\odot}^2 F_{\odot} = 4\pi R^2 F \tag{3.1}$$

with

$R_\odot = 6,956.10^8\ m$ : solar radius

$F_\odot = 6,45.10^7\ W.m^{-2}$ : energy flow of the surface of the sun

$R \in [2.06644,\ 2.49228].10^{11}\ m$ : distance Mars-Sun (Aphelion and Perihelion)

$$F = F_\odot \left(\frac{R_\odot}{R}\right)^2 \in [502, 730]\ W/m^2 \tag{3.2}$$

In this report, we will consider that the rover is working on a specific date and we will chose the one when $R$ corresponds to the semi-major axis. In this case $R = 2,27936.10^{11}\ km$ and

$$F = 589\ W/m^2 \tag{3.3}$$

Moreover, we can assume that a part of the irradiance is absorbed by the atmosphere. Knowing that the atmosphere of Earth absorbs and scatters to space around 30% of the incident irradiance of the Sun[9], and knowing that the atmosphere of Mars is thinner than the one of the Earth, we will postulate that 10% of the incident irradiance is absorbed. Thus, using (3.3) the actual irradiance $F_a$ of the light from the sun falling on the surface of Mars is

$$F_a = \frac{90}{100}F = \frac{90 * 589}{100} = 530\ W/m^2 \tag{3.4}$$

However, this irradiance is the one of surface exposed perpendicular to the sun's beams. As Mars is a sphere, the projection need to be considered. Knowing that the weather is better into the northern hemisphere of Mars[8] and the fact that a latitude between 30 an 70 degrees is favored for a landing[2], we will assume that the rover has a latitude of 50°. This latitude corresponds to an angle of 40° between the surface of Mars and the sun's beams. Moreover, suppose that the rover stop working when this angle is inferior to 10°. Thus, the irradiance $F_{50}$ at a latitude of 50° is

$$F_{50} = F_a \sin(angleBeams) \in [92, 341]\ W/m^2 \tag{3.5}$$

with $angleBeams = [10, 90 - latitude] = [10, 40]°$.

### 3.1.6 Target's Radiance

Considering the trajectory of the Sun into the sky of Mars and knowing that the rock target is more or less vertical to the surface of Mars, the angle $\theta$ between the target's normal and the sun's beam is considered to be included in $[10, 50]°$. In addition, in the optimal case (when all the optimal conditions are provided to have the maximal radiance), the BRDF of the surface of the target is assumed to be 90% Lambertian and 10% Glossy while in the worst case the BRDF will be only Lambertian. In this way, the radiance of the target $R_T$ is

$$R_T = \begin{cases} \frac{F_{50}\alpha}{\pi}\cos\theta & \text{optimal case} \\ F_{50}\alpha(\frac{9}{10\pi}\cos\theta + \frac{1}{10}) & \text{worst case} \end{cases} \tag{3.6}$$

with

$\alpha \in [0.05, 0.45]$, the albedo of the target2.1.1

$\theta \in [10, 50]°$, the angle between the target's normal and the sun's beam

Thus,

$$R_T \in [1.44, 58.58]\ W/m^2 \tag{3.7}$$

### 3.1.7 Target's Irradiance

Now, the irradiance of the target $I_T$ can be calculated with

$$I_T = R_T \frac{\pi}{4}\left(\frac{Dsr}{EFL}\right)^2 \cos(\alpha_{CT})^4 \tag{3.8}$$

with

$\alpha_{CT}$ the angle between the normal of the target and the axis of the camera

$Dsr$ the effective lens entrance aperture

$EFL$ the focal length

However, knowing that the camera is supposed to be right in front of the target, we have

$\alpha_{CT} = 0$

And according to (3.8), (3.7), 3.1.4 and 3.1.3, we have

$$I_T \in [0.0271, 1.1000]\ W/m^2 \tag{3.9}$$

Finally, the luminous power from the target to the camera per pixel $W_{lum}$ is

$$W_{lum} = I_T P_s \tag{3.10}$$

with

$P_s = 12.10^{-6}.10^{-6}\ m^2$, the pixel size of the CCD

According to (3.9)

$$W_{lum} \in [3.900, 158.40].10^{-10}\ W \tag{3.11}$$

### 3.1.8 Signal/Noise Ratio

Three different cases will be studied. In the first one, we examine the case of a target iluminated by the sun without the use of laser, the second one considers the use of lasers by night and the last one, which is the case that we need to consider for our rover, study the use of lasers by daylight. In order to calculate the Signal/Noise ratio, the different noises need to be determined. Three will be taken into account: the readout noise, the dark current noise and the noise from the sun light.

The three different cases have the readout and the dark current noise in common which are given by the datasheet of the CCD B.

$$\delta_{readout} = \frac{RMS}{N_{pixel}} \tag{3.12}$$

$$= 2,3842.10^{-05}\ el/pixel \tag{3.13}$$

$$\delta_{dark} = \left(2,55.10^{15} N_{dc0} T_s (P_s.10^2)^2 T^{\frac{2}{3}} e^{-\frac{E_g}{2kT}}\right)^{\frac{1}{2}} \tag{3.14}$$

$$= 0.0067\ el/pixel \tag{3.15}$$

with

$RMS = 25\ el$, the RMS readout noise B

$N_{pixel} = 1024\ pixels$, the number of pixel of the CCDB

$N_{dc0} = 30\ pA/cm^2$, the dark current level at 20°C B

$T_s = 0.1\ s$, the shutter time

$P_s = 12.10^{-6}\ m$, the pixel size B

$T = 197\ K$, the temperature

$E_g = 1.1557 - \frac{7.10^{-4}T^2}{1108+T}$

$k = 8,62.10^{-5}\ eV/K$, the Boltzmann's constant

#### 3.1.8.1 First case

In this case, the signal that needs to be considered is the sun light reflected by the target. Therefore, the readout and the dark current noises are the only two which need to be considered and the noise is

$$N = \sqrt{\delta_{readout}^2 + \delta_{dark}^2} = 0.0067\ el/pixel \tag{3.16}$$

Then, the number of photons per shutter time $N_p$ corresponding o the radiance of the target is

$$N_p = \frac{1}{\lambda_{max} - \lambda_{min}} \int_{\lambda_{min}}^{\lambda_{max}} \frac{W_{lum} ts}{\frac{h.c}{\lambda}} \mathrm{d}\lambda \in [1.177, 47.810].10^6\ photons/pixel \tag{3.17}$$

with

$ts = 0.1\ s$, shutter time

$h = 6,6263.10^{-}34\ J.s$, Planck's constant

$c = 3.10^{8}\ m/s$, velocity of light

$\lambda \in [400, 800]\ nm$, wavelength of the sunlight

The number of photons per pixel going to the lens $N_{CCD}$ is

$$N_{CCD} = \frac{\pi \left(\frac{Dsr}{2}\right)^2}{2\pi(r)^2} N_p \in [0.1328, 5.3936]\ photons/pixel \tag{3.18}$$

with $r = 2\ m$, the distance between the camera and the target
The number of photons per pixel to the lens registered by the CCD $Nen_{CCD}$ is

$$Nen_{CCD} = N_{CCD} \int_{\lambda_{min}}^{\lambda_{max}} CCDqe(\lambda).alphaLens(\lambda)\, \mathrm{d}\lambda \in [0.0208, 0.8457]\, photons/pixel \tag{3.19}$$

with

$CCDqe$, the quantum efficiency of the CCD 2.1

$alphaLens$, the pass band efficiency of the lens

Finally, according to (3.16) and (3.19) we obtain the Signal/Noise ratio

$$\frac{S}{N} = \frac{Nen_{CCD}}{N} = [3.1, 126.8] \tag{3.20}$$

Knowing that, 100 is a really great Signal/Noise ratio, we can conclude that the system could record images of satisfactory or high quality the most of the time. However, if the different poor conditions accumulate, the quality of the image will greatly decrease.

#### 3.1.8.2 Second case

In this case, the signal that needs to be considered is the light of the pseudo laser reflected by the target. Therefore, the noise is still the same as in the first case.

Proceeding in the same way as with the we did with the sunlight and using (**??**), the number of photons per pixel $Nen_{LED}$ from the artificial light source going toward the CCD is

$$Nen_{LED} = [2.4556, 26.9410]\ photon/pixel \tag{3.21}$$

And the Signal/Noise ratio is given by

$$\frac{S}{N} = \frac{Nen_{LED}}{N} = [368, 4040]\ photon/pixel \tag{3.22}$$

# Appendix A

# LED Properties

### Caractéristiques

| | |
|---|---|
| • Couleur | Vert |
| • Température de couleur | 525nm |
| • Intensité Lumineuse | 84000mcd |
| • Ampérage Requis | 20mA |
| • Angle de Diffusion | 30° |
| • Consommation | 220mW |
| • Tension d'alimentation | 9.3 - 10.5V |
| • Durée de vie estimée | 80 000 Heures |

Figure A.1: LED Datasheet

# Appendix B

# CCD Properties

# DATA SHEET

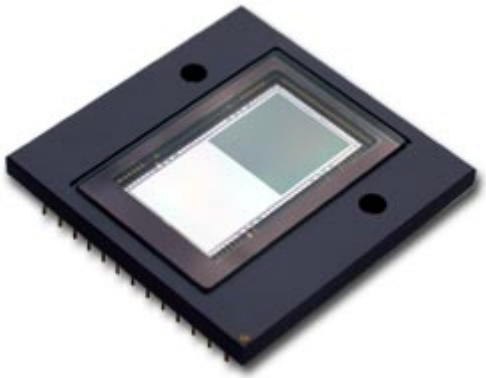

# FTT1010M

## 1M Frame Transfer CCD Image Sensor

Product specification

2007, April 17

**DALSA**
**Professional Imaging**

# 1M Frame Transfer CCD Image Sensor FTT1010M

- **1-inch optical format**
- **1M active pixels (1024H x 1024V)**
- **Progressive scan**
- **Excellent antiblooming**
- **Variable electronic shuttering**
- **Square pixel structure**
- **H and V binning**
- **100% fill factor**
- **High dynamic range (>72dB)**
- **High sensitivity**
- **Low dark current and fixed pattern noise**
- **Low readout noise**
- **Data rate up to 2 x 40 MHz**
- **Mirrored and split readout**
- **RoHS compliant**

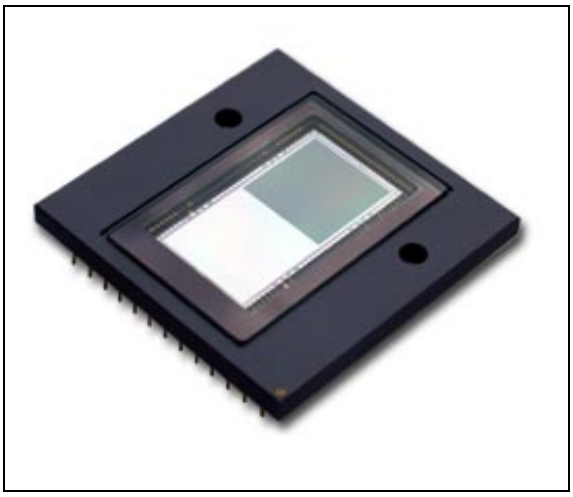

## Description

The FTT1010M is a monochrome progressive-scan frame-transfer image sensor offering 1K x 1K pixels at 30 frames per second through a single output buffer. The combination of high speed and a high linear dynamic range (>12 true bits at room temperature without cooling) makes this device the perfect solution for high-end real time medical X-ray, scientific and industrial applications. A second output can either be used for mirrored images, or can be read out simultaneously with other output to double the frame rate. The device structure is shown in figure 1.

## Device structure

| | |
|---|---|
| Optical size: | 12.288 mm (H) x 12.288 mm (V) |
| Chip size: | 14.572 mm (H) x 26.508 mm (V) |
| Pixel size: | 12 $\mu$m x 12 $\mu$m |
| Active pixels: | 1024 (H) x 1024 (V) |
| Total no. of pixels: | 1072 (H) x 1030 (V) |
| Optical black pixels: | Left: 20 Right:20 |
| Timing pixels: | Left: 4 Right:4 |
| Dummy register pixels: | Left: 7 Right: 7 |
| Optical black lines: | Bottom: 6 Top: 6 |

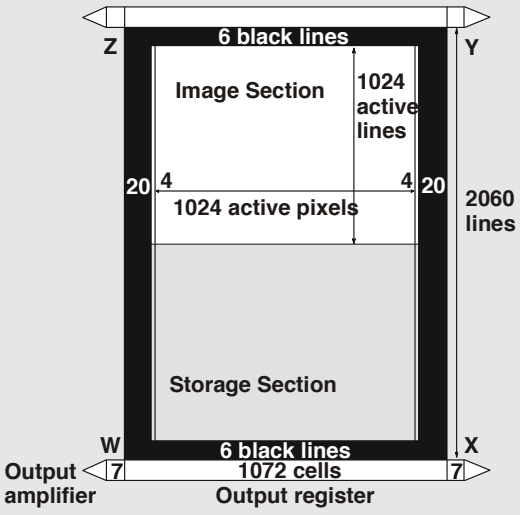


**Figure 1 – Device Structure**

## Architecture of the FTT1010M

The FTT1010M consists of a shielded storage section and an open image section. Both sections are electronically the same and have the same cell structure with the same properties. The only difference between two sections is the optical light shield.

The optical centres of all pixels in the image section form a square grid. The charge is generated and integrated in this section. Output registers are located below the storage section. The output amplifiers Y and Z are not used in Frame Transfer mode and should be connected as not-used amplifiers.

After the integration time, the charge collected in the image section is shifted to the storage section. The charge is read out line by line through the lower output register.

The left and the right half of each output register can be controlled independently. This enables either single or multiple readout.

During vertical transport, the C3 gates separate the pixels in the register. The letters W, X, Y, and Z are used to define the four quadrants of the sensor. The central C3 gates of both registers are part of the W and Z quadrants of the sensor.

Both upper and lower registers can be used for vertical binning. Both registers also have a summing gate at each end that can be used for horizontal binning. Figure 2 shows the detailed internal structure.

| **IMAGE SECTION** | |
|---|---|
| Image diagonal (active video only) | 17.38 mm |
| Aspect ratio | 1:1 |
| Active image width x height | 12.288 x 12.288 $mm^2$ |
| Pixel width x height | 12 x 12 $\mu m^2$ |
| Fill factor | 100% |
| Image clock pins | A1, A2, A3, A4 |
| Capacity of each clock phase | 2.5nF per pin |
| Number of active lines | 1024 |
| Number of black reference lines | 6 |
| Total number of lines | 1030 |
| Number of active pixels per line | 1024 |
| Number of overscan (timing) pixels per line | 8 (2x4) |
| Number of black reference pixels per line | 40 (2x20) |
| Total number of pixels per line | 1072 |

| **STORAGE SECTION** | |
|---|---|
| Storage width x height | 12.864 x 12.360 $mm^2$ |
| Cell width x height | 12 x 12 $\mu m^2$ |
| Storage clock phases | B1, B2, B3, B4 |
| Capacity of each clock phase | 2.5nF per pin |
| Number of cells per line | 1072 |
| Number of lines | 1030 |

| **OUTPUT REGISTERS** | |
|---|---|
| Output buffers (three-stage source follower) | 4 (one on each corner) |
| Number of registers | 2 (one above, one below) |
| Number of dummy cells per register | 14 (2x7) |
| Number of register cells per register | 1072 |
| Output register horizontal transport clock pins | C1, C2, C3 |
| Capacity of each C-clock phase | 60pF per pin |
| Overlap capacity between neighbouring C-clocks | 20pF |
| Output register Summing Gates | 4 pins (SG) |
| Capacity of each SG | 15pF |
| Reset Gate clock phases | 4 pins (RG) |
| Capacity of each RG | 15pF |

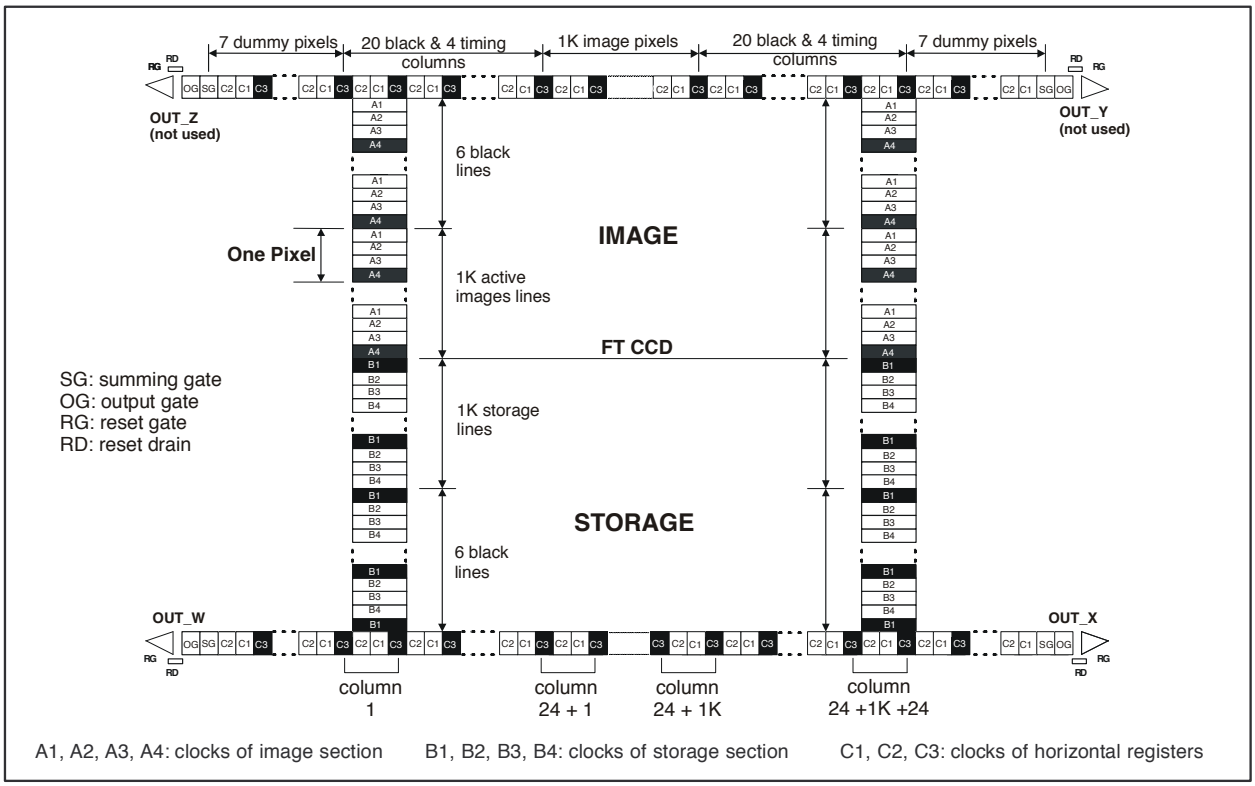


**Figure 2 - Detailed internal structure**

Specifications

| ABSOLUTE MAXIMUM RATINGS[1] | MIN | MAX | UNIT |
|---|---|---|---|
| GENERAL: | | | |
| storage temperature | -55 | +80 | °C |
| ambient temperature during operation | -40 | +60 | °C |
| voltage between any two gates | -20 | +20 | V |
| DC current through any clock (absolute value) | -0.2 | +0.2 | μA |
| OUT current (no short circuit protection) | 0 | 10 | mA |
| VOLTAGES IN RELATION TO VPS: | | | |
| VPS, SFD, RD | -0.5 | +30 | V |
| VCS, SFS | -8 | +5 | V |
| All other pins | -5 | +25 | V |
| VOLTAGES IN RELATION TO VNS: | | | |
| SFD, RD | -15 | +0.5 | V |
| VCS, SFS, VPS | -30 | +0.5 | V |
| All other pins | -30 | +0.5 | V |

| DC CONDITIONS[2,3] | | MIN [V] | TYPICAL [V] | MAX [V] | MAX [mA] |
|---|---|---|---|---|---|
| VNS[4] | N substrate | 20 | 24 | 28 | 15 |
| VPS | P substrate | 1 | 3 | 7 | 15 |
| SFD | Source Follower Drain | 16 | 20 | 24 | 4.5 |
| SFS | Source Follower Source | - | 0 | - | 1 |
| VCS | Current Source | -5 | 0 | 3 | _ |
| OG | Output Gate | 4 | 6 | 8 | _ |
| RD | Reset Drain | 13 | 15.5 | 18 | _ |

| AC CLOCK LEVEL CONDITIONS[2] | MIN | TYPICAL | MAX | UNIT |
|---|---|---|---|---|
| IMAGE CLOCKS: | | | | |
| A-clock amplitude during integration and hold | 8 | 10 | | V |
| A-clock amplitude during vertical transport (duty cycle=5/8) [5] | 10 | 14 | | V |
| A-clock low level | | 0 | | V |
| Charge Reset (CR) level on A-clock[6] | -5 | -5 | | V |
| STORAGE CLOCKS: | | | | |
| B-clock amplitude during hold | 8 | 10 | | V |
| B-clock amplitude during vertical transport (duty cycle=5/8) | 10 | 14 | | V |
| OUTPUT REGISTER CLOCKS: | | | | |
| C-clock amplitude (duty cycle during hor. transport=3/6) | 4.75 | 5 | 5.25 | V |
| C-clock low level | 2 | 3.5 | | V |
| Summing Gate (SG) amplitude | | 10 | 10 | V |
| Summing Gate (SG) low level | | 3.5 | | V |
| OTHER CLOCKS: | | | | |
| Reset Gate (RG) amplitude | 5 | 10 | 10 | V |
| Reset Gate (RG) low level | | 3 | | V |
| Charge Reset (CR) pulse on Nsub[6] | 0 | 10 | 10 | V |

[1] During Charge Reset it is allowed to exceed maximum rating levels (see note 5)
[2] All voltages in relation to SFS
[3] Power-up sequence: VNS, SFD, RD, VPS, others
[4] To set the VNS voltage for optimal Vertical Antiblooming (VAB), it should be adjustable between minimum and maximum values
[5] Three-level clock is preferred for maximum charge; the swing during vertical transport should be 4V higher than the voltage during integration
A two level clock (typically 10V) can be used if a lower maximum charge handling capacity is allowed
[6] Charge Reset can be achieved in two ways:
• The typical CR level is applied to all image clocks simultaneously (preferred).
• The typical A-clock low level is applied to all image clocks; for proper CR, an additional Charge Reset pulse on VNS is required. This will also affect the charge handling capacity in the storage areas.

### Timing diagrams (for default operation)

| AC CHARACTERISTICS | MIN | TYPICAL | MAX | UNIT |
|---|---|---|---|---|
| Horizontal frequency (1/Tp)[1] | 0 | 18 | 40 | MHz |
| Vertical frequency | 0 | 450 | 1000 | kHz |
| Charge Reset (CR) time | 2 | 20 | | $\mu$s |
| Rise and fall times: image clocks (A) | 10 | 20 | | ns |
| storage clocks (B) | 10 | 20 | | ns |
| register clocks (C)[2] | 3 | 5 | 1/6 Tp | ns |
| summing gate (SG) | 3 | 5 | 1/6 Tp | ns |
| reset gate (RG) | 3 | 5 | 1/6 Tp | ns |

[1] TP=1 clock period
[2] Duty cycle=50% and phase shift of the C clocks is 120 degrees

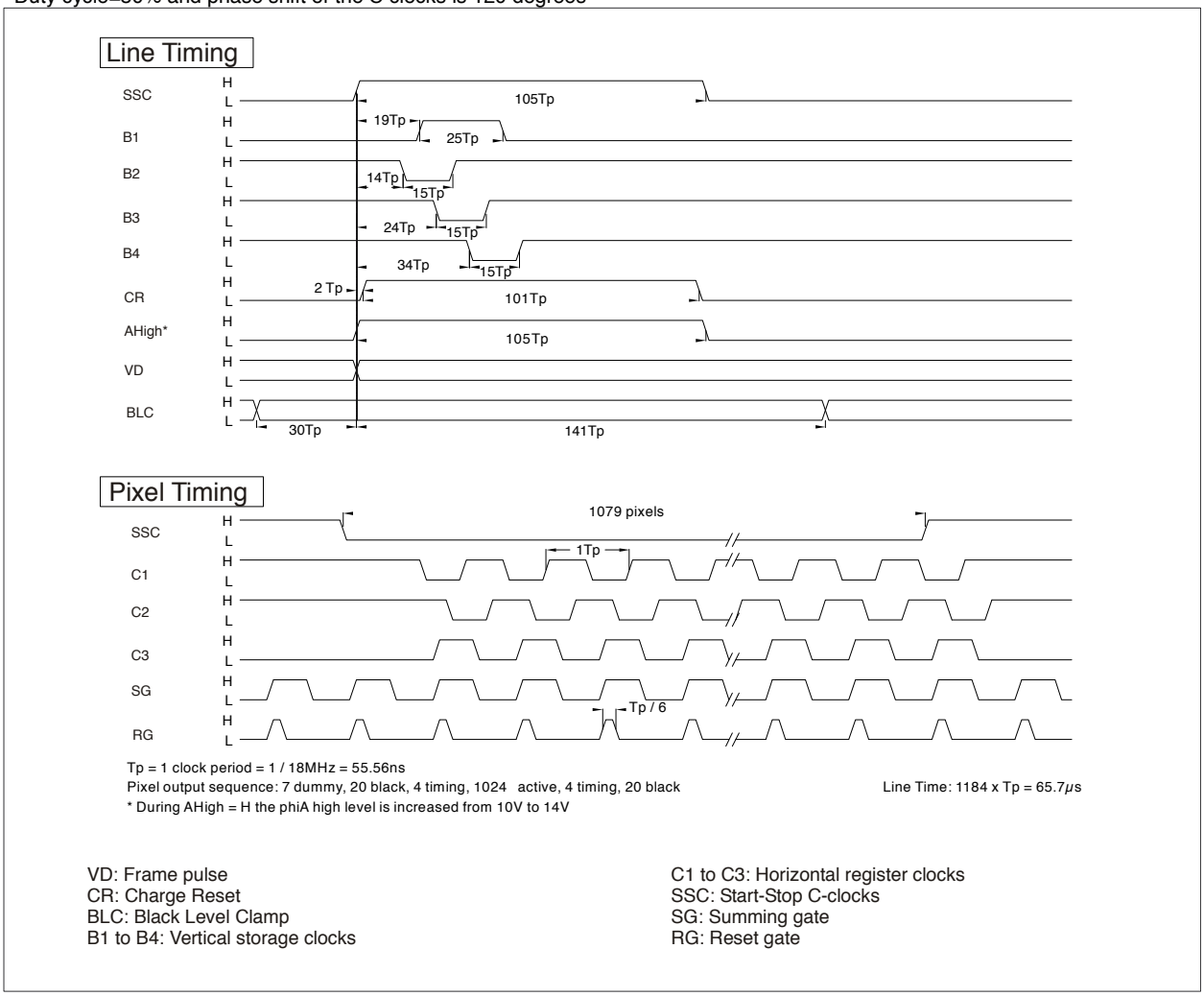


**Figure 3 - Line and pixel timing diagrams**

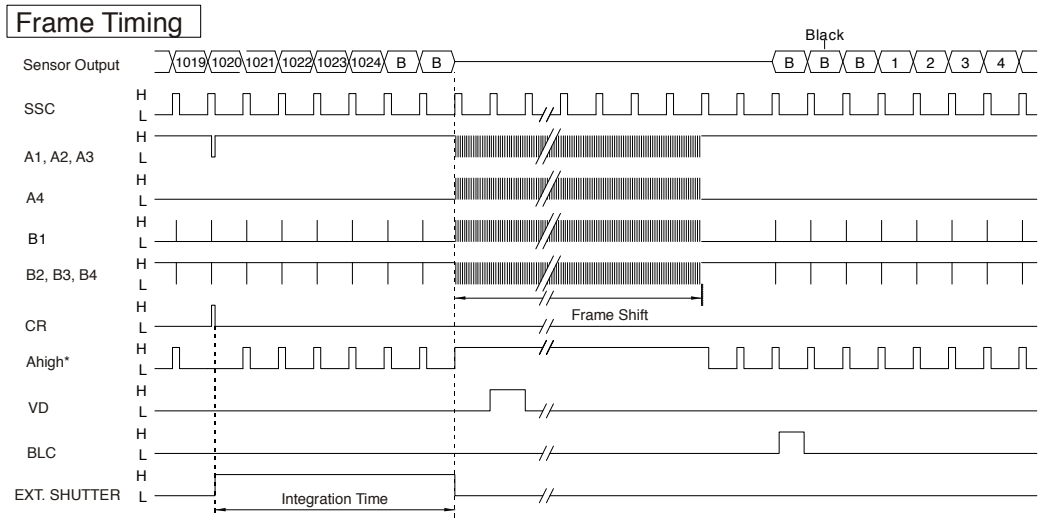


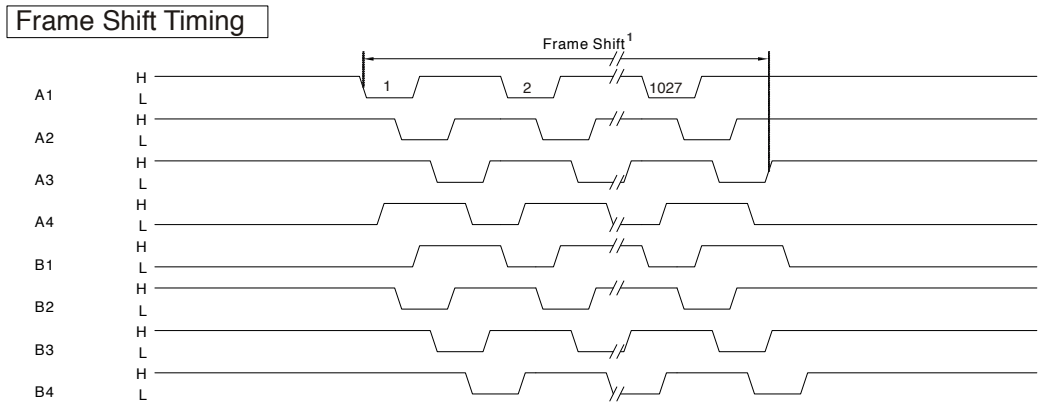


[1] Line periods needed for Frameshift $N = \frac{1027}{\text{Linetime x Vertical Frequency}} = 35$

VD: Frame pulse
CR: Charge Reset
BLC: Black Level CLamp
A1 to A4: Vetical Image clocks

B1 to B4: Vertical storage clocks
C1 to C3: Horizontal register clocks
SSC: Start-Stop C-clocks
SG: Summing gate
RG: Reset gate

**Figure 4 - Frame timing diagrams**

**Line timing**

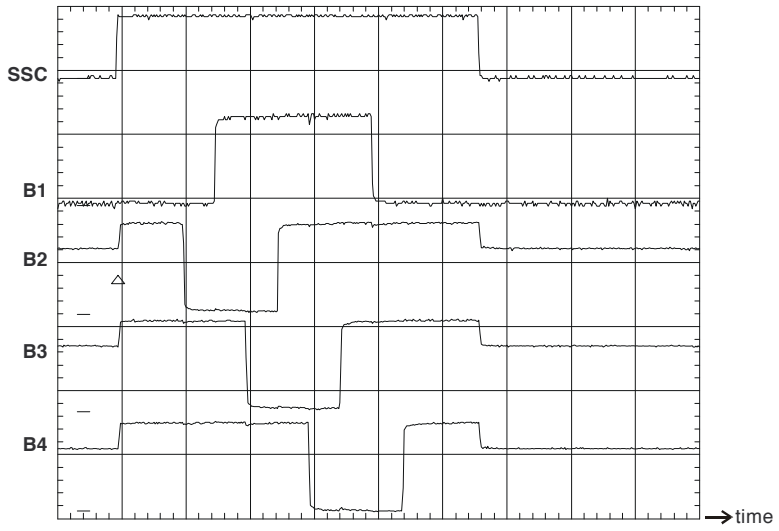


Y/Div. : 10V (B1, B2, B3, B4); 5V (SSC)

**Figure 5 - Vertical readout**

**Pixel timing**

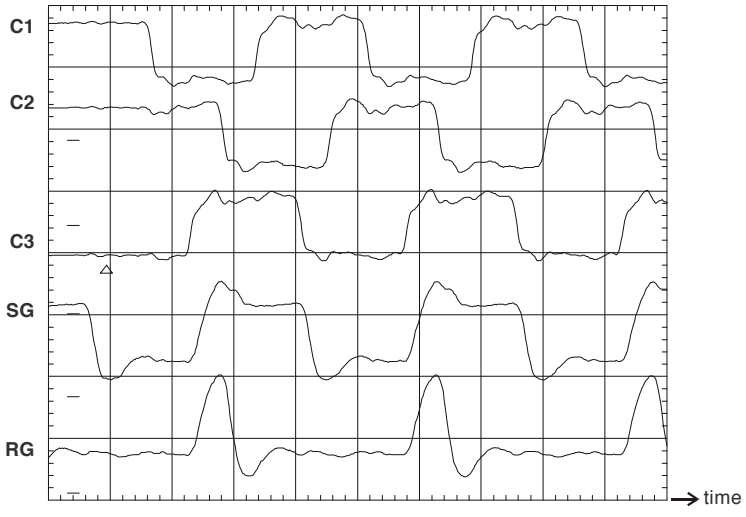


Y/Div. : 5V (C1, C2, C3); 10V (SG, RG)

**Figure 6 - Start horizontal readout**

## Performance

The test conditions for the performance characteristics are as follows:

- All values are measured using typical operating conditions.
- VNS is adjusted as low as possible while maintaining proper Vertical Antiblooming
- Sensor temperature=60°C (333K)
- Horizontal transport frequency=18MHz
- Vertical transport frequency=450kHz
- Integration time=10ms
- The light source is a lamp of 3200K in conjunction with neutral density filters and a 1.7mm thick BG40 infrared cut-off filter. For Linear Operation measurements, a temperature conversion filter (Melles Griot type no. 03FCG261, -120 mired, thickness: 2.5mm) is applied.

.

| LINEAR OPERATION | MIN | TYPICAL | MAX | UNIT |
|---|---|---|---|---|
| Charge Transfer Efficiency[1] vertical | | 0.999995 | | |
| Charge Transfer Efficiency[1] horizontal | | 0.999999 | | |
| Image lag | | | 0 | % |
| Smear[2] | | -39 | 0 | dB |
| Resolution (MTF) @ 42lp/mm | 65 | | | % |
| Light sensitivity | 180 | 250 | | kel/lux•s |
| Low Pass Shading[3] | | | 2.5 | % |
| Random Non-Uniformity (RNU)[4] | | 0.3 | 5 | % |

[1]Charge Transfer Efficiency values are tested by evaluation and expressed as the value per gate transfer.
[2]Smear is defined as the ratio of 10% of the vertical transport time to the integration time. It indicates how visible a spot of 10% of the image height would become.
[3]Low Pass Shading is defined as the ratio of the one-σ value of the pixel output distribution expressed as a percentage of the mean value output (low-pass image).
[4]RNU is defined as the ratio of the one-σ value of the highpass image to the mean signal value at nominal light.

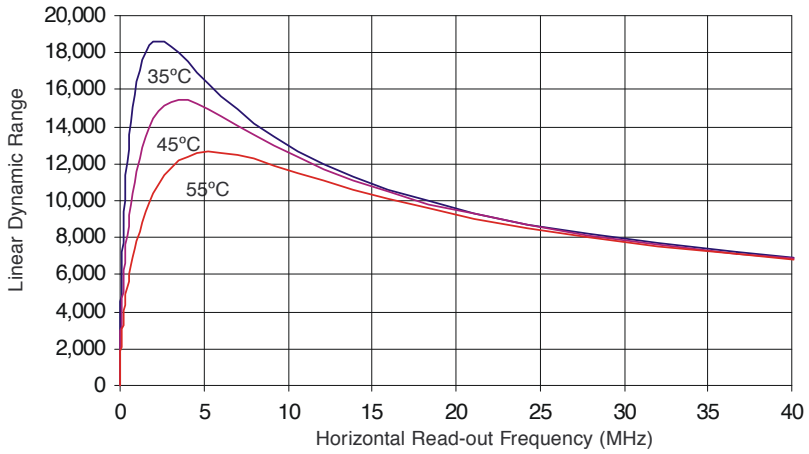


Linear dynamic range is defined as the ratio of $Q_{lin}$ to read-out noise (the latter reduced by Correlated Double Sampling).

**Figure 7 - Typical Linear dynamic range vs. horizontal read-out frequency and sensor temperature**

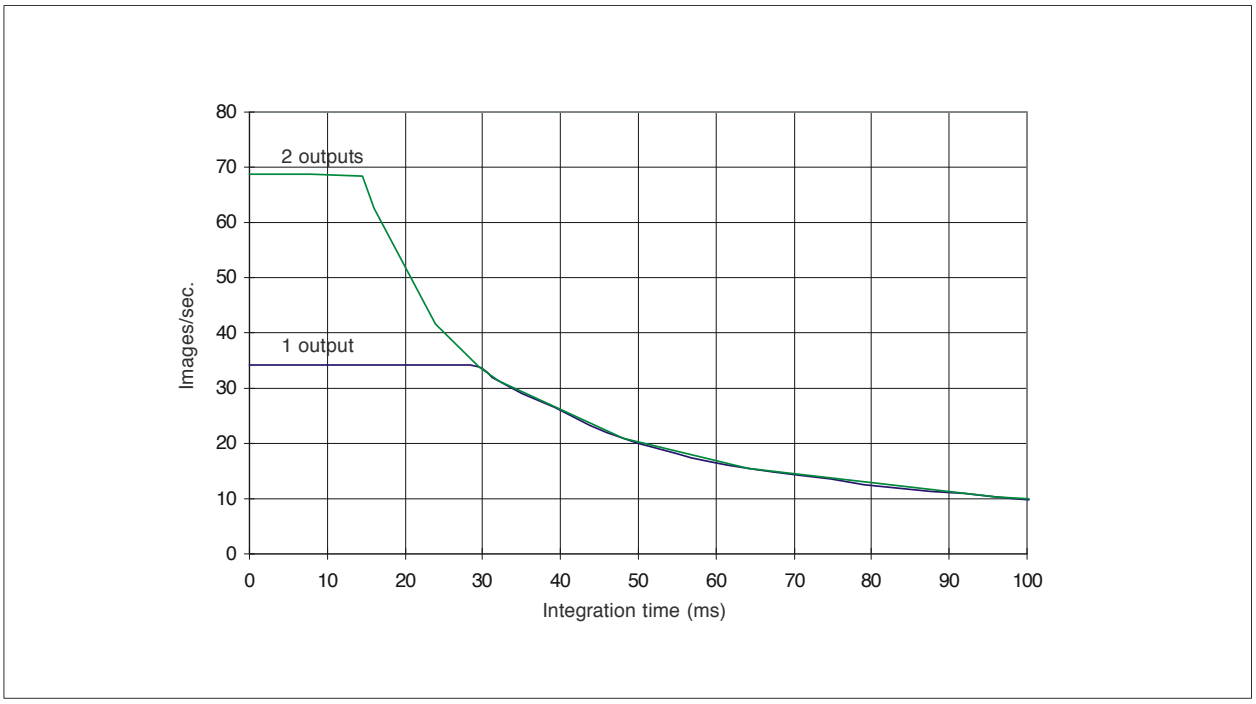


**Figure 8 - Maximum number of images/second versus integration time**

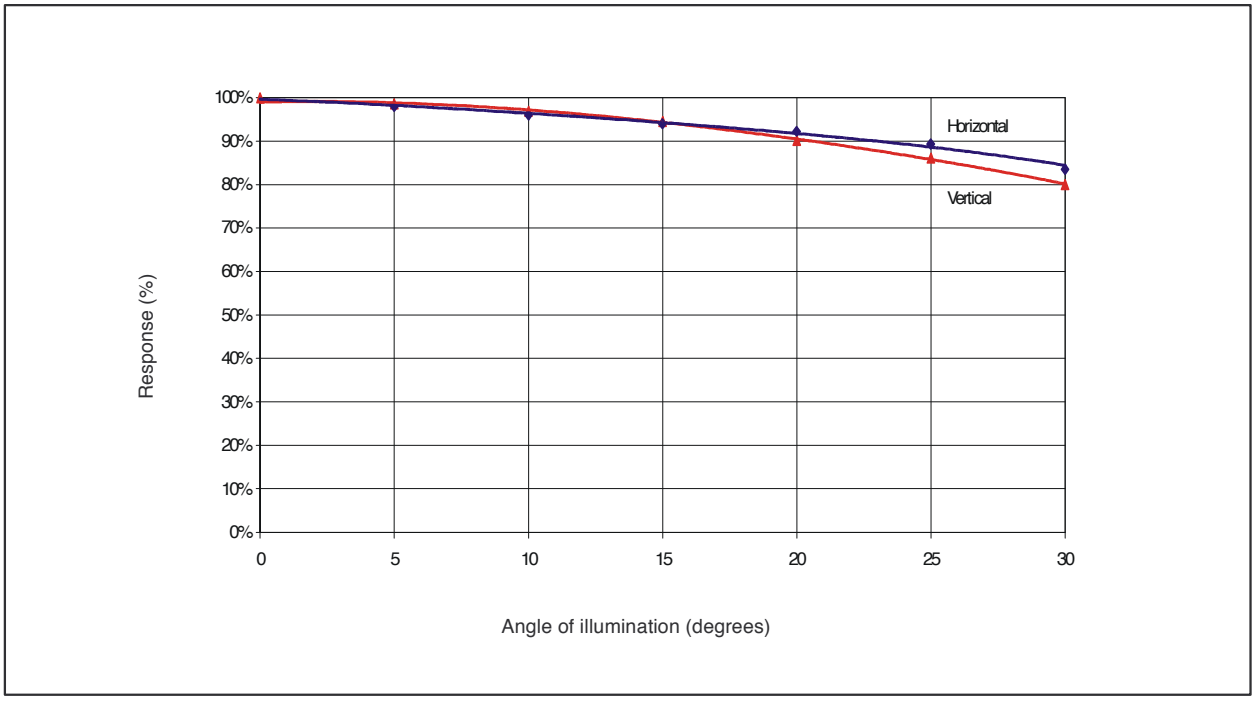


**Figure 9 - Angular response versus angle of illumination**

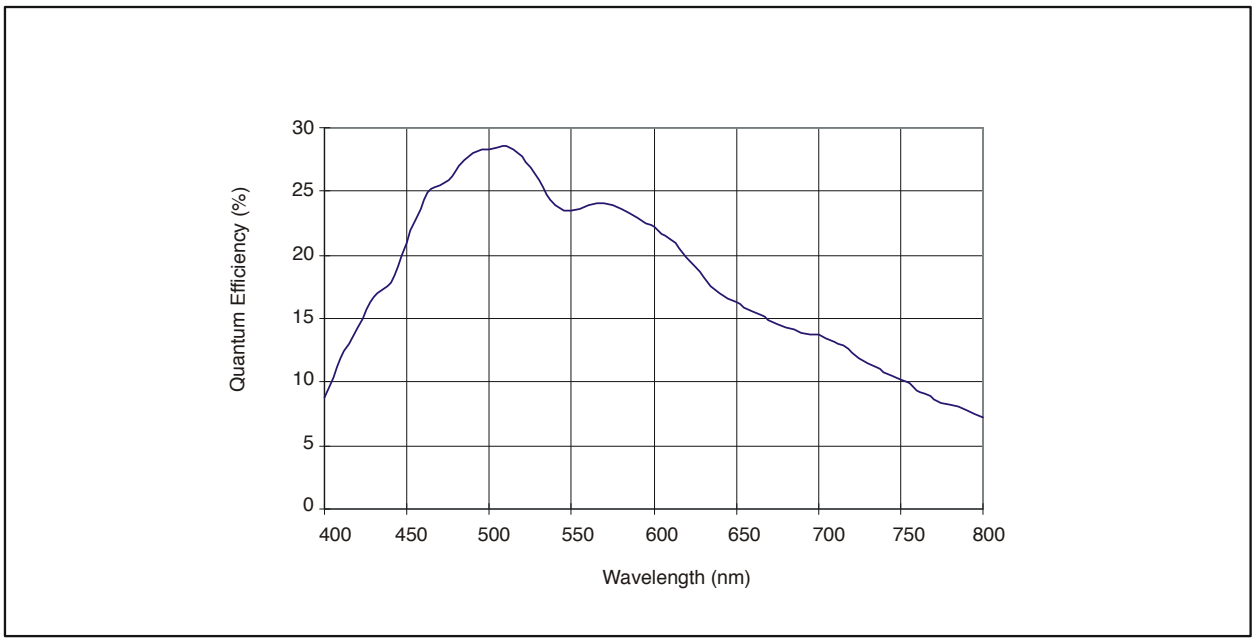


**Figure 10 - Quantum efficiency versus wavelength**

| LINEAR/SATURATION | MIN | TYPICAL | MAX | UNIT |
|---|---|---|---|---|
| Full-well capacity saturation level (Qmax)[1] | 250 | 500 | 600 | kel |
| Full-well capacity linear operation (Qlin)[2] | 200 | 350 | | kel |
| Charge handling capacity[3] | | 600 | | kel |
| Overexposure[4] handling | 100 | 200 | | x Qmax level |

[1]Qmax is determined from the low-pass filtered image.
[2]The linear full-well capacity Qlin is calculated from linearity test (see dynamic range). The evaluation test guarantees 97% linearity.
[3]Charge handling capacity is the largest charge packet that can be transported through the register and read-out through the output buffer.
[4]Overexposure over entire area while maintaining good Vertical Antiblooming (VAB). It is tested by measuring the dark line.

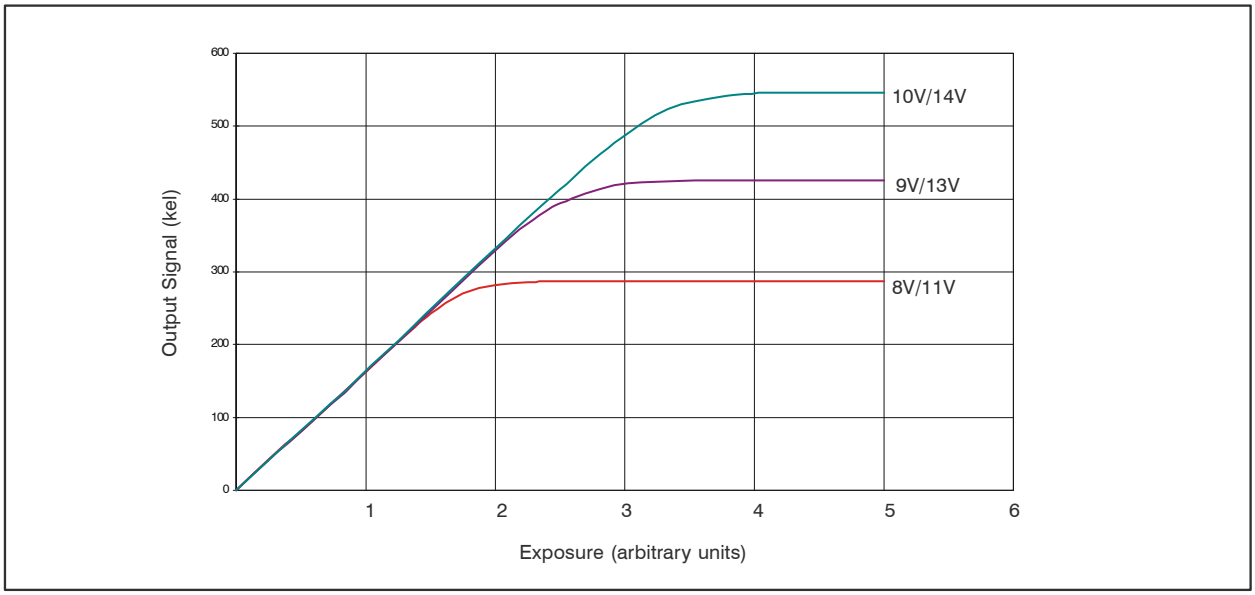


**Figure 11 – Charge handling versus integration/transport voltage**

| OUTPUT BUFFERS | MIN | TYPICAL | MAX | UNIT |
|---|---|---|---|---|
| Conversion factor | 6 | 8 | 12 | $\mu$V/el |
| Mutual conversion factor matching ($\Delta$ACF)[1] | | 0 | 2 | $\mu$V/el |
| Supply current | | 4 | | mA |
| Bandwidth | | 110 | | MHz |
| Output impedance buffer ($R_{load}$=3.3$\Omega$, $C_{load}$=2pF) | | 400 | | $\Omega$ |

[1]Matching of the four outputs is specified as $\Delta$ACF with respect to reference measured at the operating point ($Q_{lin}$/2)

| DARK CONDITION | MIN | TYPICAL | MAX | UNIT |
|---|---|---|---|---|
| Dark current level @ 20°C | | 10 | 30 | pA/cm$^2$ |
| Dark current level @ 60°C | | 0.3 | 0.6 | nA/cm$^2$ |
| Fixed Pattern Noise[1] (FPN) @ 60ºC | | 15 | 25 | el |
| RMS readout noise @ 9MHz bandwidth after CDS | | 25 | 30 | el |

[1]FPN is one-$\sigma$ value of the high-pass image.

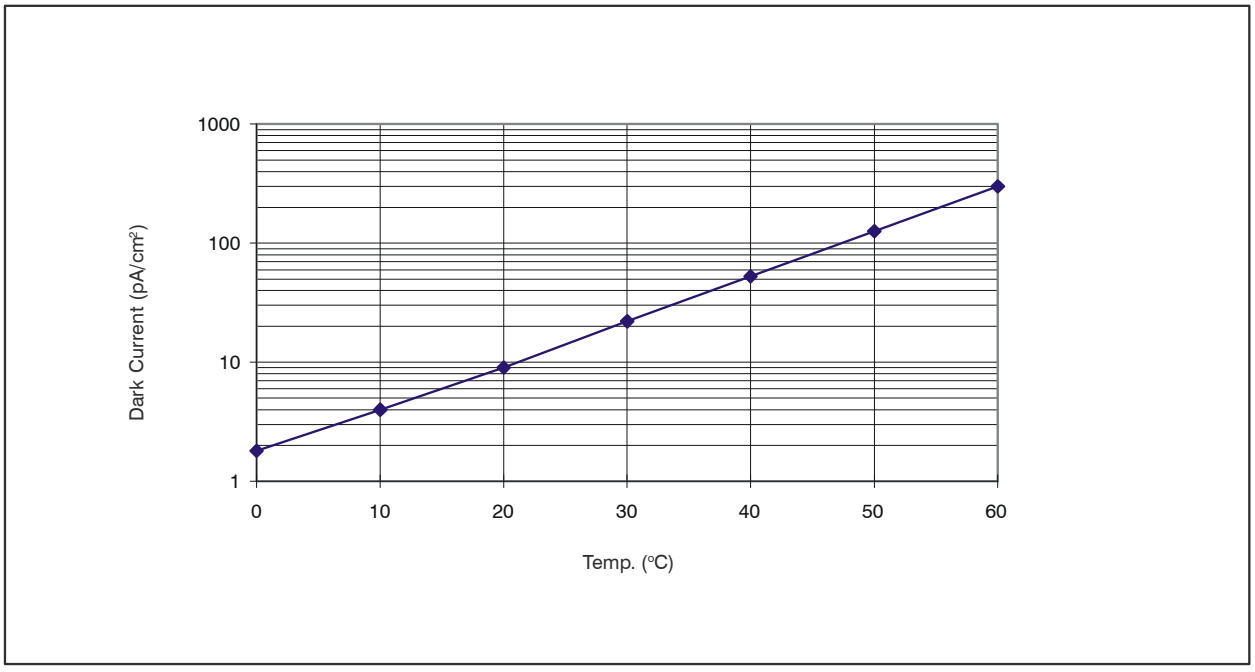


**Figure 12 – Dark current versus temperature**

## Application information

*Current handling*
One of the purposes of VPS is to drain the holes that are generated during exposure of the sensor to light. Free electrons are either transported to the VRD connection and, if excessive (from overexposure), free electrons are drained to VNS. No current should flow into any VPS connection of the sensor. During high overexposure a total current of 10 to 15mA through all VPS connections together may be expected. The PNP emitter follower in the circuit diagram (figure 12) serves these current requirements.

VNS drains superfluous electrons as a result of overexposure. In other words, it only sinks current. During high overexposure, a total current of 10 to 15mA through all VNS connections together may be expected. The clamp circuit, consisting of the diode and electrolytic capacitor, enables the addition of a Charge Reset (CR) pulse on top of an otherwise stable VNS voltage. To protect the CCD, the current resulting from this pulse should be limited. This can be accomplished by designing a pulse generator with a rather high output impedance.

*Decoupling of DC voltages*
All DC voltages (not VNS, which has additional CR pulses as described above) should be decoupled with a 100nF decoupling capacitor. This capacitor must be mounted as close as possible to the sensor pin. Further noise reduction (by bandwidth limiting) is achieved by the resistors in the connections between the sensor and its voltage supplies. The electrons that build up the charge packets that will reach the floating diffusions only add up to a small current, which will float through VRD. Therefore, a large series resistor in the VRD connection may be used.

*Outputs*
To limit the on-chip power dissipation, the output buffers are designed with open source outputs. Outputs to be used should therefore be loaded with a current source or more simply with a resistance to GND. In order to prevent the output (which typically has an output impedance of about 400Ω) from bandwidth limitation as a result of capacitive loading, load the output with an emitter follower built from a high-frequency transistor. Mount the base of this transistor as close as possible to the sensor and keep the connection between the emitter and the next stage short. The CCD output buffer can easily be destroyed by ESD. By using this emitter follower, this danger is suppressed; do NOT reintroduce this danger by measuring directly on the output pin of the sensor with an oscilloscope probe. Instead, measure on the output of the emitter follower. Slew rate limitation is avoided by avoiding a too-small quiescent current in the emitter follower; about 10mA should do the job. The collector of the emitter follower should be decoupled properly to suppress the Miller effect from the base-collector capacitance.

A CCD output load resistor of 3.3Ω typically results in a bandwidth of 110MHz. The bandwidth can be enlarged to about 130MHz by using a resistor of 2.2kΩ instead, which, however, also enlarges the on-chip power dissipation.

*Device protection*
The output buffers of the FTT1010M are likely to be damaged if VPS rises above SFD or RD at any time. This danger is most realistic during power-on or power-off of the camera. The RD voltage should always be lower than the SFD voltage.

Never exceed the maximum output current. This may damage the device permanently. The maximum output current should be limited to 10mA. Be especially aware that the output buffers of these image sensors are very sensitive to ESD damage.

Because of the fact that our CCDs are built on an n-type substrate, we are dealing with some parasitic npn transistors. To avoid activation of these transistors during switch-on and switch-off of the camera, we recommend the application diagram of figure 12.

*Unused sections*
To reduce power consumption, the following steps can be taken. Connect unused output register pins (C1...C3, SG, OG) and unused SFS pins to zero Volts.

*More information*
Detailed application information is provided in the application note AN01 entitled “**Camera Electronics for the mK x nK CCD Image Sensor Family**”.

## Device Handling

An image sensor is a MOS device which can be destroyed by electro-static discharge (ESD). Therefore, the device should be handled with care.

Always store the device with short-circuiting clamps or on conductive foam. Always switch off all electric signals when inserting or removing the sensor into or from a camera (the ESD protection in the CCD image sensor process is less effective than the ESD protection of standard CMOS circuits).

Being a high quality optical device, it is important that the cover glass remain undamaged. When handling the sensor, use fingercots.

When cleaning the glass we recommend using ethanol (or possibly water). Use of other liquids is strongly discouraged:

- if the cleaning liquid evaporates too quickly, rubbing is likely to cause ESD damage.
- the cover glass and its coating can be damaged by other liquids.

Rub the window carefully and slowly.

Dry rubbing of the window may cause electro-static charges or scratches which can destroy the device.

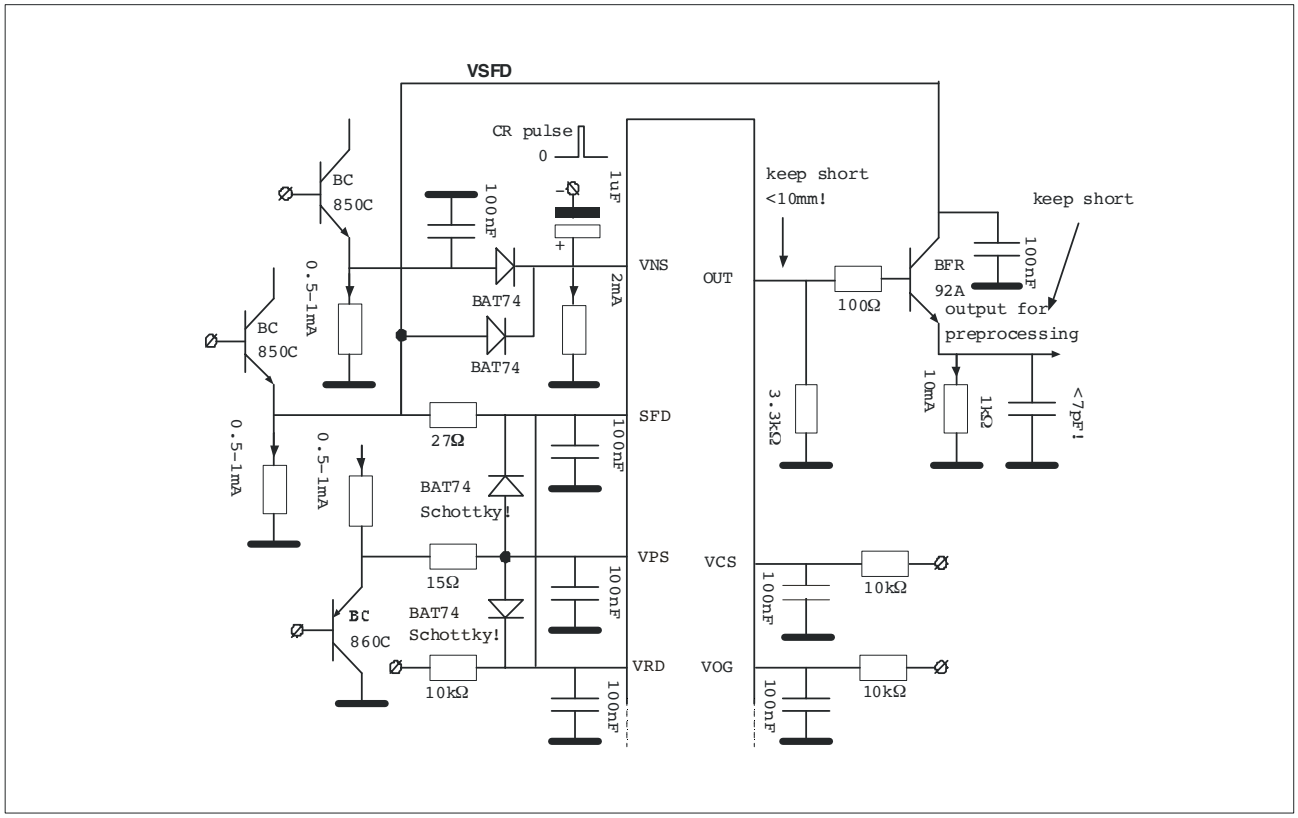


**Figure 13– Application diagram**

## Pin configuration

The FTT1010M is mounted in a Pin Grid Array (PGA) package with 80 pins in a 15x13 grid of 40.00 x 40.00 $mm^2$. The position of pin A1 is marked with a gold dot on top of the package. The image clock phases of quadrant W are internally connected to X, and the clock phases of Y are connected to Z.

| SYMBOL | LINEAR/SATURATION | PIN # W | PIN # X | PIN # Y | PIN # Z |
|---|---|---|---|---|---|
| VNS | N substrate | A12 | A3 | J2 | F11 |
| VNS | N substrate | D11 | B2 | F3 | H12 |
| VNS | N substrate | E11 | D3 | - | J11 |
| VNS | N substrate | E12 | E2 | - | - |
| VNS | N substrate | - | E3 | - | - |
| VPS | P substrate | C11 | C3 | G3 | G11 |
| SFD | Source Follower Drain | A13 | A1 | J1 | J13 |
| SFS | Source Follower Source | A10 | B5 | J4 | H9 |
| VCS | Current Source | A11 | A4 | J3 | J10 |
| OG | Output Gate | B13 | B1 | H1 | H13 |
| RD | Reset Drain | B12 | B3 | H2 | H11 |
| A1 | Image Clock (Phase 1) | - | - | F1 | F13 |
| A2 | Image Clock (Phase 2) | - | - | G2 | G12 |
| A3 | Image Clock (Phase 3) | - | - | F2 | F12 |
| A4 | Image Clock (Phase 4) | - | - | G1 | G13 |
| B1 | Storage Clock (Phase 1) | D13 | D1 | - | - |
| B2 | Storage Clock (Phase 2) | C12 | C2 | - | - |
| B3 | Storage Clock (Phase 3) | D12 | D2 | - | - |
| B4 | Storage Clock (Phase 4) | C13 | C1 | - | - |
| C1 | Register Clock (Phase 1) | B9 | A6 | H5 | J8 |
| C2 | Register Clock (Phase 2) | B8 | A7 | H6 | J7 |
| C3 | Register Clock (Phase 3) | A8 | B6 | J6 | H8 |
| SG | Summing Gate | B10 | A2 | H4 | J12 |
| RG | Reset Gate | A9 | A5 | J5 | J9 |
| OUT | Output | B11 | B4 | H3 | H10 |
| NC | Not Connected | B7 | | H7 | |

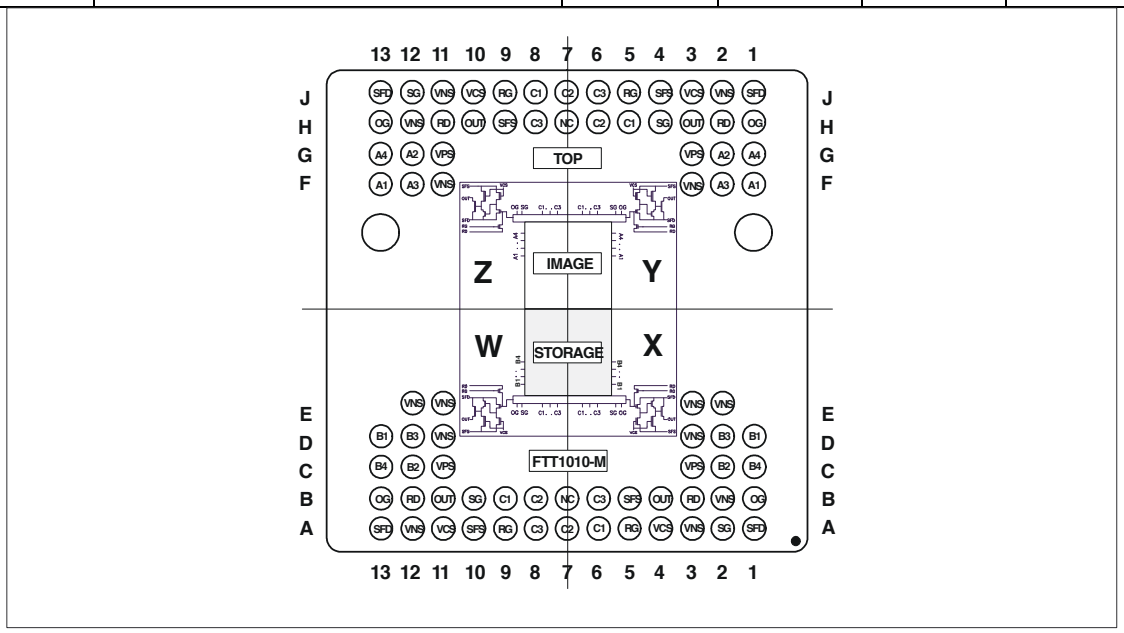


**Figure 14 - Pin configuration (top view)**

**Package information**

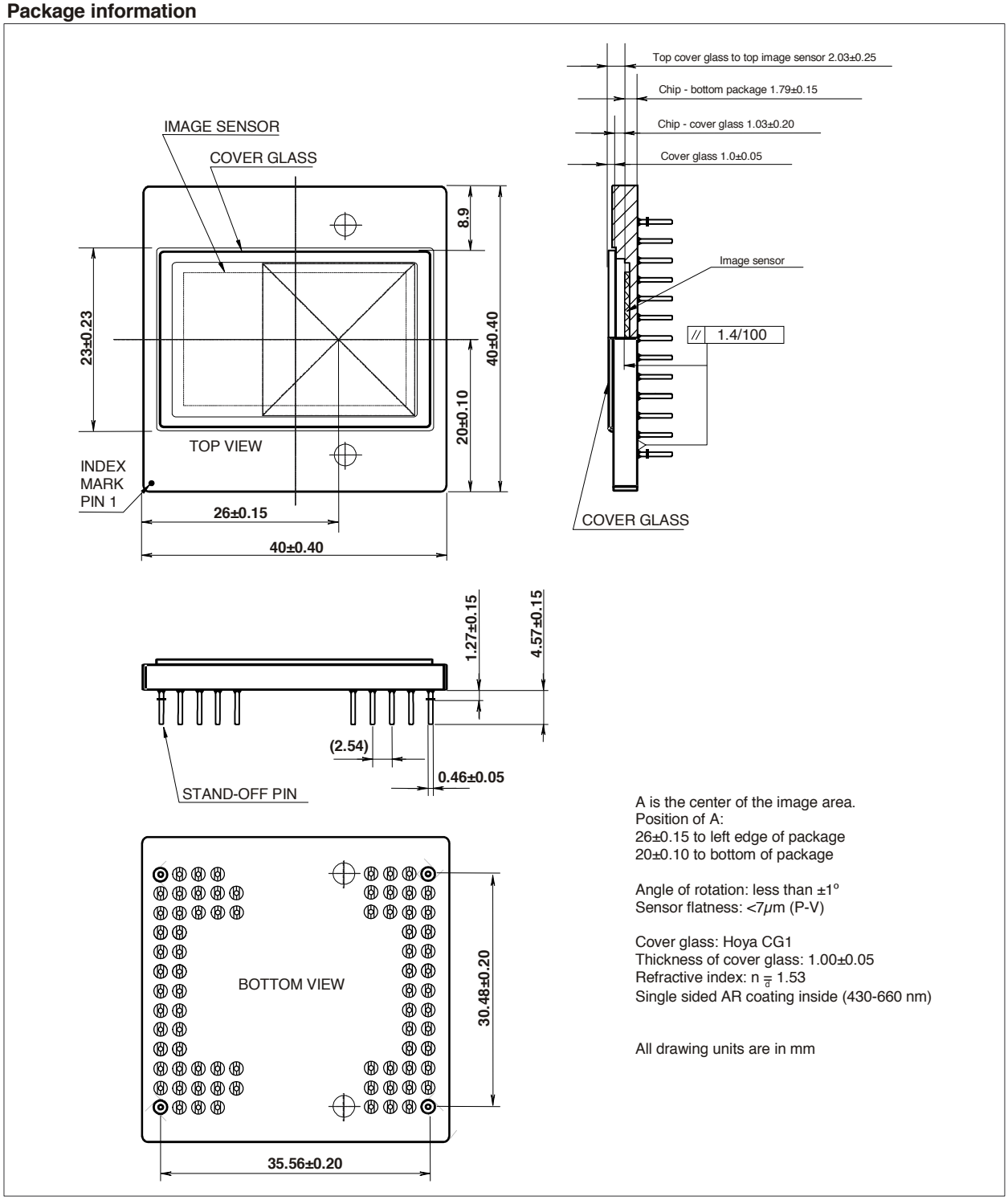


**Figure 15– Mechanical drawing of the PGA package of the FTT1010M**

## Order codes

The sensor can be ordered using the following code:

| FTT1010M sensors | | |
|---|---|---|
| **Description** | **Quality Grade** | **Order Code** |
| FTT1010M/TG | Test grade | 9922 157 35231 |
| FTT1010M/EG | Economy grade | 9922 157 35251 |
| FTT1010M/IG | Industrial grade | 9922 157 35221 |
| FTT1010M/HG | High grade | 9922 157 35211 |


### Defect Specifications

The CCD image sensor can be ordered in a specific quality grade. The grading is defined with the maximum amount of pixel defects, column defects, row defects and cluster defects, in both illuminated and non-illuminated conditions. For detailed grading information, please contact your local DALSA representative.

## For More Information

For more detailed information on this and other products, contact your local rep or visit our Web site at http://www.dalsa.com/sensors/products/products.asp.

**DALSA Professional Imaging**
Sales Department
High Tech Campus 27
5656 AE Eindhoven
The Netherlands
Tel: +31 40 259 9009
Fax: +31 40 259 9015
www.dalsa.com/sensors
sales.sensors@dalsa.com

**This information is subject to change without notice.**

# Bibliography


[1] Berthold Horn. *Robot vision*. MIT press, 1986.

[2] John Leif Jørgensen, 2015.

[3] Hubert H Lamb. Climate present past and future vol-1. 1975.

[4] JN Maki, JF Bell, KE Herkenhoff, SW Squyres, A Kiely, M Klimesh, M Schwochert, T Litwin, R Willson, A Johnson, et al. Mars exploration rover engineering cameras. *Journal of Geophysical Research: Planets (1991–2012)*, 108(E12), 2003.

[5] NASA. Robotic mars exploration, 2015. [Online; accessed November 25, 2015].

[6] Wikipedia. Atmosphère de mars — Wikipedia, the free encyclopedia, 2015. [Online; accessed November 25, 2015].

[7] Wikipedia. Circle of confusion — wikipedia, the free encyclopedia, 2015. [Online; accessed November 25, 2015].

[8] Wikipedia. Mars — Wikipedia, the free encyclopedia, 2015. [Online; accessed November 25, 2015].

[9] Giichi Yamamoto. Direct absorption of solar radiation by atmospheric water vapor, carbon dioxide and molecular oxygen. *Journal of the Atmospheric Sciences*, 19(2):182–188, 1962.